Differential Phase Patterns of the LOFAR LBA Array Measured In Situ

Fabio Paonessa[1], Giuseppe Virone[1], Stefania Matteoli[1], Pietro Bolli[2], Giuseppe Pupillo[3], Stefan J. Wijnholds[4]
[1] Istituto di Elettronica e di Ingegneria dell'Informazione e delle Telecomunicazioni (IEIIT), Consiglio Nazionale delle Ricerche (CNR), Torino, Italy, giuseppe.virone@ieiit.cnr.it, fabio.paonessa@ieiit.cnr.it
[2] Osservatorio Astrofisico di Arcetri (OAA), Istituto Nazionale di Astrofisica (INAF), Firenze, Italy, pbolli@arcetri.inaf.it
[3] Istituto di Radioastronomia (IRA), Istituto Nazionale di Astrofisica (INAF), Bologna, Italy, g.pupillo@ira.inaf.it
[4] Netherlands Institute for Radio Astronomy (ASTRON), Dwingeloo, The Netherlands, wijnholds@astron.nl

***Abstract*—A complete electromagnetic model for an antenna array describes both the amplitude and phase of the embedded element patterns. The predicted phase response can usually be validated with an experimental setup in which the transmitting source is phase-locked with the receiving system. This is unpractical or even unfeasible in certain situations, such as in the case of a test source mounted on an Unmanned Aerial Vehicle (UAV) used for in-situ validation of low-frequency radio astronomical arrays. In this paper, we exploit the phase difference between the received signals to further validate the array EM models. We applied this method on a subarray of the Low Frequency Array (LOFAR).**

Index Terms—antenna arrays, antenna measurements, phased arrays, radio astronomy, unmanned aerial vehicles (UAVs)

I. Introduction

The Low Frequency Array (LOFAR) [1] radio telescope consists of several stations (subarrays) spread over Europe, each of them composed of two subarrays of Low-Band Antennas (LBAs) and High-Band Antennas (HBAs) operating in the frequency bands 10–90 MHz and 120–240 MHz, respectively.

First experimental tests on LOFAR stations were done exploiting astronomical calibration sources [2] and artificial sources [3]. More recently, UAV-mounted artificial sources have been further developed and tested on a number of isolated antennas [4],[5] and small arrays [6]-[8] with good results. In March 2016, this measurement solution was exploited on a single LOFAR station (subarray of the full LOFAR, see Fig. 1). The main aim of the campaign was to perform in-situ validation of the array electromagnetic model. The description of the campaign and some preliminary results have already been reported in [9]. Besides providing valuable data for the validation of the embedded-element amplitude patterns, the UAV-based system has been used to measure the differential phase patterns, i.e. the difference between the phase patterns of two elements within the array, as well. Both the procedure and the main results are discussed in this paper.

Fig. 1. Partial view of the LBA array. The UAV equipped with a 2-m long dipole is taking off

II. Differential Phase Patterns

The LOFAR digital backend has been set up to record the voltages at the output ports of an LBA station configuration during the flight of the UAV-mounted test source. The signals from the individual antennas are digitized and split into narrowband channels using a polyphaser filter bank. The time series output of this filter bank can be recorded for the selected channels.

In this measurement setup, the source is not phase-locked to the receiver. Therefore, the absolute phase values are affected by the drift of the two different reference oscillators. As a consequence, phase pattern measurements cannot be performed. However, differential phase patterns with respect to a reference element are sufficient to completely characterize the radiation pattern of the overall array as well as for EM model validation.

One array element is selected as phase reference. The difference between the phase ϕ_i of the complex signal acquired from the i-th element and the phase ϕ_R of the reference one is measured by correlating the individual time series. All the time varying quantities $\phi_i - \phi_R$ have been synchronized with the GPS clock. The test source position is also known with the same time reference. Therefore, the $\phi_i - \phi_R$ can be expressed as a function of

the test source position. This dependence is hereafter understood and therefore not mentioned explicitly.

The UAV-mounted test source can perform constant-height flights above the array. However, it cannot always satisfy the far-field condition. Therefore, each array element is generally illuminated at a different angle from the source (parallax effect). It means that the measured differential phase shift $\phi_i - \phi_R$,

$$\phi_i - \phi_R = -K(R_i - R_R) + \lfloor M_i - \lfloor M_R \qquad (1)$$

is a function of both the differential propagation phase $K(R_i - R_R)$ (where K is the propagation constant and R_i and R_R are the distance between the i-th element and the source and between the reference and the source, respectively) and the phase difference between the polarization mismatch factors M_i and M_R [4]. It should be remembered that the latter

$$\begin{aligned} \lfloor M_i &= \phi_i^{AUT} + \phi_i^S \\ \lfloor M_R &= \phi_R^{AUT} + \phi_R^S \end{aligned} \qquad (2)$$

contain both the relevant embedded-element phase pattern values ϕ_i^{AUT} and ϕ_R^{AUT} and the source pattern values ϕ_i^S and ϕ_R^S. Again, the source pattern value ϕ_i^S and ϕ_R^S, seen from the considered element and the reference one, respectively, are different from each other in the radiating near-field region (parallax effect). As far as ϕ_i^{AUT} and ϕ_R^{AUT} are concerned, it should be noted that they are different also in the far-field, owing to the different element position inside the array.

The relevant differential phase patterns $\phi_i^{AUT} - \phi_R^{AUT}$ are hence obtained from the measured $\phi_i - \phi_R$ by removing both the differential propagation phase and the other differential source contribution

$$\phi_i^{AUT} - \phi_R^{AUT} = \phi_i - \phi_R + K(R_i - R_R) - (\phi_i^S - \phi_R^S) \qquad (3)$$

where R_i and R_R are obtained from the measured position of the source, whereas ϕ_i^S and ϕ_R^S also requires knowledge of both the UAV orientation and the source model [10].

III. Experimental Results

Four flights were performed along the E-plane of the LBAs oriented North-East. This direction is represented with the dashed magenta line in Fig. 2 along with the LBA inner element distribution of a LOFAR station. The considered array size is about 30 m. Therefore, the far-field distance is about 350 m at 57 MHz. One flight was performed at 300 m i.e. approaching the far-field condition. Three additional flights were performed at a height of 100 m. These trajectories clearly fall in the radiating near-field region of the 30-m array, however, they could have been considered as sufficient to reach the far-field condition as far as the embedded-element patterns

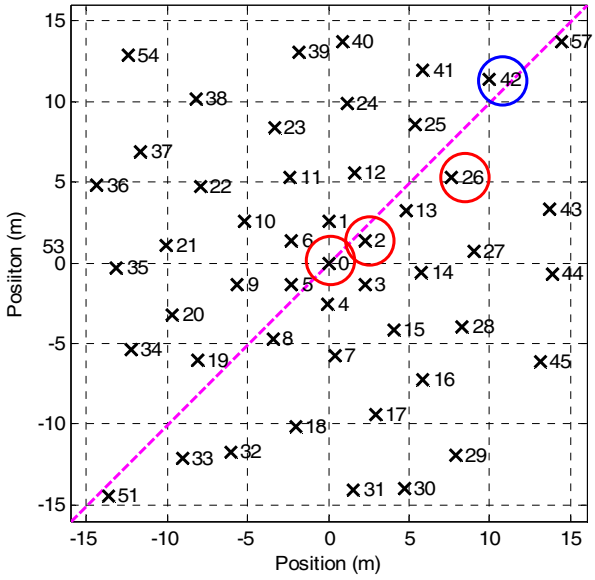

Fig. 2. Inner element distribution of LBA elements within a LOFAR station.

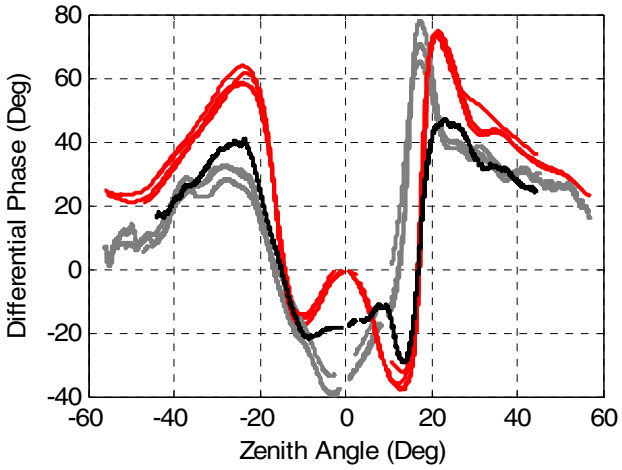

Fig. 3. Differential phase patterns between element 0 and element 42 at 57 MHz. Measurement in quasi far-field condition (black curve) and near-field measurements (grey curves) are compared with simulations (red curves).

are concerned. As a matter of fact, a diameter-of-influence of about 15 m was estimated from preliminary simulations of such a random sparse array configuration.

The measured differential phase shift between the central element (#0 in Fig. 2) and the selected reference (#42 in Fig. 2) has been processed according to (3). Element #42 has been selected as reference because it is quite far from the center, where strong mutual coupling effects are expected. The results for both the quasi far-field and the near-field flights are shown in Fig. 3, with the black and grey lines, respectively. There is good consistency between the near-field traces (grey lines). However, the far-field data exhibit a quite different

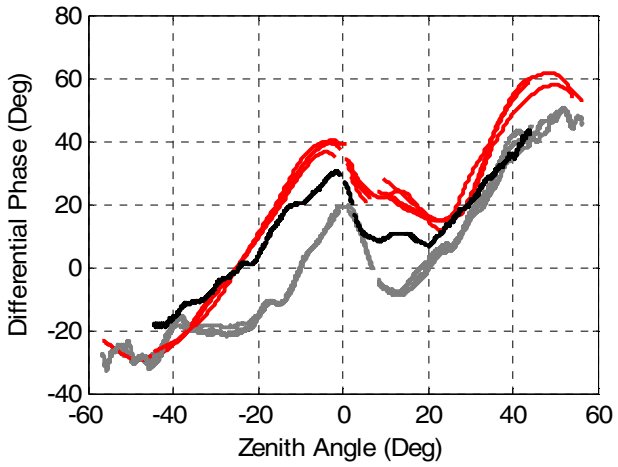

Fig. 4. Differential phase patterns between element 2 and element 42 at 57 MHz. Measurement in quasi far-field condition (black curve) and near-field measurements (grey curves) are compared with simulations (red curves).

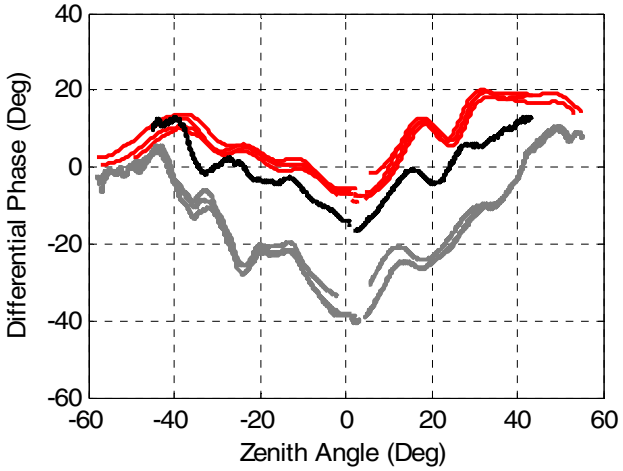

Fig. 5. Differential phase patterns between element 26 and element 42 at 57 MHz. Measurement in quasi far-field condition (black curve) and near-field measurements (grey curves) are compared with simulations (red curves).

behavior from the near-field ones. These discrepancies have been explained by further numerical simulations showing that at 57 MHz the mutual coupling between the array elements is higher than expected. As a matter of fact, 57 MHz is the resonance frequency of the LBA element (including the amplifier). At this frequency, the diameter-of-influence is actually even larger than 30 m.

The simulated differential phase patterns are also shown in Fig. 3 with the red lines. The curves are slightly different to each other because these simulations were performed considering the real trajectories of the UAV [4]. The adopted simulation model exploited far-field embedded-element patterns. As expected, it provides a closer agreement with the measured data in the quasi far-field condition. It is possible to simulate the actual transfer function between individual antennas and a source in the radiating near-field of the array. It is expected that the agreement between measurements and simulations can be improved further by such simulations.

Similar considerations apply for the differential phase patterns of elements #2 and #26, which are reported in Figs. 4 and 5, respectively. These elements exhibit smoother behavior with respect to the central one. However, element #2 is still very different from a dipole-like pattern. They are less affected by mutual coupling phenomena because the average element spacing is increasing towards the array boundary (see Fig. 2). As expected, near-field and far-field measured data are more similar for these elements.

It should be noted that a phase offset is always present between measurements (black curves) and simulations (red curves). This discrepancy is entirely related to the phase calibration of the receiving chain. For each element, the phase offset visible in Figs. 3–5 has been estimated by minimizing the RMS difference between the quasi far-field measurement and the corresponding simulation. Both the estimated offset values and the associated residuals are

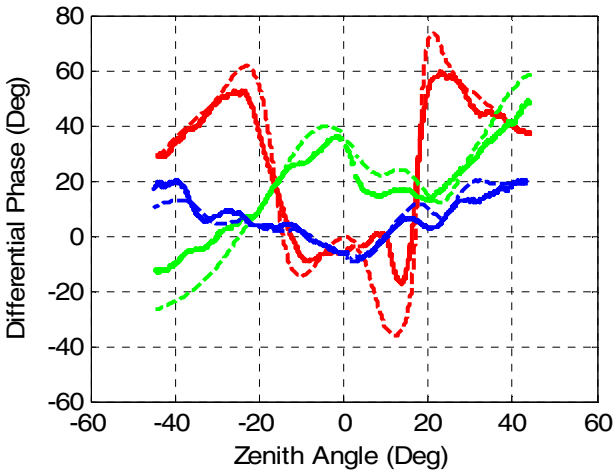

Fig. 6. Differential phase patterns between elements 0 (red), 2 (green), 26 (blue) and element 42 at 57 MHz: simulation (dashed line), meaurement with applied phase offet (solid line).

reported in Table I. Fig. 6 shows the quasi far-field measurements with applied phase offsets (solid lines) in good agreement with the corresponding simulations (dashed lines).

TABLE I. COMPUTED PHASE OFFSETS AND RMS RESIDUALS

Element n.	Reference element	Computed Offset	RMS after correction
0	42	12.4°	9.6°
2	42	5.9°	8.5°
26	42	7.1°	3.64°

IV. CONCLUSIONS

The phase difference between the received signals at element level has been exploited to further validate the EM models of the LOFAR LBA inner subarray. A good agreement has been observed in the quasi far-field condition of the UAV-mounted test source.

Constant phase offsets between measurements and simulations have been estimated within the element field-of-view by minimizing the RMS difference between measurement and simulation. These values are entirely related to the residual phase differences between the RF chains that should be calibrated out. Therefore, the presented procedure can be also considered as a possible calibration refinement tool for digitally-beam-formed phased arrays.

ACKNOWLEDGMENT

The authors thank Menno Norden and Michel Arts from ASTRON, Paolo Maschio, Irene Aicardi and Horea Bendea from Politecnico di Torino (DIATI), and Augusto Olivieri from CNR-IEIIT for their valuable technical contribution to the experimental activity.

This work was partially supported by the Italian National Institute for Astrophysics under the TECNO INAF 2014 program and by the Netherlands Organization for Scientific Research.

REFERENCES

[1] M. P. van Haarlem et al, "LOFAR: The LOw-Frequency ARray", Astronomy & Astrophysics, vol. 556, A2, 1-53, Aug. 2013.

[2] S. J. Wijnholds and W. A. van Cappellen, "In Situ Antenna Performance Evaluation of the LOFAR Phased Array Radio Telescope", IEEE Trasn. on Antennas and Propagat., Vol. 59, No. 6, June 2011

[3] A. Nelles, et al, "Calibrating the absolute amplitude scale for air showers measured at LOFAR", JINST 10 (2015) no.11, P11005 arXiv:1507.08932

[4] G. Virone, et al., "Antenna pattern verification system based on a micro unmanned aerial vehicle (UAV)," IEEE Antennas and Wireless Propagation Letters, vol.13, pp. 169-172, Jan. 2014.

[5] P. Bolli, et al, "Antenna pattern characterization of the low-frequency receptor of LOFAR by means of an UAV-mounted artificial test source", SPIE Astronomical Telescopes and Instrumentation, Edinburgh, United Kingdom, 26 June - 1 July 2016

[6] G. Pupillo, et al., "Medicina array demonstrator: calibration and radiation pattern characterization using a UAV-mounted radio-frequency source," Experimental Astronomy, vol. 39, pp. 405-421, Apr. 2015.

[7] P. Bolli, et al. "From MAD to SAD: The Italian experience for the low-frequency aperture array of SKA1-LOW", Radio Sci., 51, 160–175, doi:10.1002/2015RS005922, Mar 2016.

[8] E. de Lera Acedo, et al., 'SKA Aperture Array Verification System: Electromagnetic modeling and beam pattern measurements using a micro UAV', accepted for publication in *Experimental Astronomy*

[9] P. Bolli, S. J. Wijnholds, E. de Lera Acedo, A. Lingua, J. Monari, F. Paonessa, G. Pupillo, G. Virone, "In-Situ Characterization of International Low-Frequency Aperture Arrays by Means of an UAV-based System", on *32nd URSI GASS, Montreal, 19-26 August 2017*

[10] G. Virone, F. Paonessa, O. A. Peverini, G. Addamo, R. Orta, R. Tascone, A. Lingua, M. Piras, P. Bolli, G. Pupillo and J. Monari, "Antenna Pattern Measurement with UAVs: Modeling of the Test Source", European Conference on Antennas and Propagation (EuCAP), Davos, Switzerland, Apr. 11-15 2016